A flute mode turbulence and a related transport in the divertor of a mirror

Isao KATANUMA[1)], Hiroshi SAIMARU[1)], Yoshinari MIZOGUCHI[1)], Katsuya YASHIRO[1)], Teruji CHO[1)] and Vladimir P. PASTUKHOV[2)]

[1)] *Plasma Research Center, University of Tsukuba, Tsukuba 305-8577, Japan*
[2)] *RRC "Kurchatov Institute", Kurchatov Square, 1, 123182 Moscow, Russia*

We investigate a flute mode turbulence and its related radial transport in a magnetic divertor. The computer code was made to simulate flute modes. This code can be applied to a magnetic shearless confinement system as well as a tandem mirror. Computer simulation carried out in a modeled magnetic divertor shows that the flute modes enhance the radial transport during its growing phase.

Keywords: divertor, flute, interchange, simulation, mirror

1. Introduction

A magnetic divertor is an application of the stable dipole magnetic configuration on a planet. And the magnetic divertor configuration has an equilibrium up to $\beta \simeq 1$, where β is the ratio of plasma pressure to the vacuum magnetic field on axis. The open magnetic confinement system such as GAMMA10 has the possibility of a fully axisymmetric system with MHD stable state by containing a magnetic divertor region.[1)]

A typical divertor magnetic field is shown in Fig.1, where the axial length $L = 200$ and a magnetic null point locates at $(r, z) = (65, 0)$. This axisymmetric mirror plasma is found to be stabilized by the plasma compressibility rather than by the ion finite Larmor radius effects around the magnetic null for the fatter radial density profiles.[2)] That is, $\partial pU^\gamma/\partial\psi > 0$ is the stability condition of plasma in Fig.1, where p is plasma pressure, $U \equiv \int \frac{d\ell}{B}$ is the specific volume of a magnetic field line, γ is the heat index and $2\pi\psi$ is the magnetic flux surrounded by the surface $\psi = const.$

The flute modes are one of the most dangerous instabilities in the magnetic shearless confinement system, so the stability analysis of the flute modes usually has a priority over other modes.[3)] However the transport process resulting from the flute instabilities has not been studied so much to the authors' knowledge. So the purpose of this paper is to investigate the flute instability and related plasma radial transport in a magnetic divertor shown in Fig.1.

As mentioned above in this paper, the flute modes are stabilized by mainly plasma compressibility in a divertor mirror cell. So that the fluid approximation can be applied to the flute mode analysis here. In the marginally stable state the plasma pressure radial profile is assumed to satisfy the relation of $pU^\gamma = const.$ Ions passing near the magnetic null region do not conserve its magnetic moment μ, which can disturb the marginally stable state, i.e. $\partial pU^\gamma/\partial\psi \lesssim 0$, where the flute modes become unstable. In the following we consider the slightly unstable state to the flute modes.

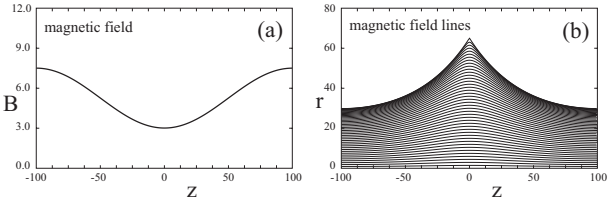

Fig. 1 Modeled magnetic divertor. (a) is axial profile of magnetic field and (b) plots magnetic field lines.

2. Basic equation

The freedom of compressible Alfvén modes and shear Alfvén modes and acoustic modes is unnecessary to calculate the flute instability, because those modes are more stable than the flute modes and that those modes usually have high frequency oscillations. One of authors (Pastukhov)[4)] has proposed a method how to remove the Alfvén modes and acoustic modes from the MHD equations, the equation of motion of which is given as

$$\frac{\partial \hat{w}}{\partial t} + [\![\Phi, \hat{w}]\!] - [\![\hat{\rho}, \langle\frac{v_\alpha^2}{2}\rangle]\!] + \frac{1}{U^\gamma}\frac{\partial U}{\partial\psi}\frac{\partial(\hat{\rho}_0\tilde{T} + \hat{T}_0\tilde{\rho})}{\partial\varphi} = UQ_w^* + \frac{3X_M}{20}\left(\frac{T_i + T_e}{2T_i}\right)\left\{\frac{\partial}{\partial\psi}\left[\hat{\rho}\langle r^2\rangle\frac{\partial}{\partial\psi}\left(\frac{1}{U^{2/3}\sqrt{\hat{T}_0}}\frac{a^2}{\langle r^2\rangle}\hat{w}\right)\right] + \frac{a^2}{\langle r^2\rangle}\left\langle\frac{1}{r^2B^2} + \lambda^2B^2\right\rangle\frac{\hat{\rho}}{U^{2/3}\sqrt{\hat{T}_0}}\frac{\partial^2\hat{w}}{\partial\varphi^2}\right\} \quad (1)$$

Here $a^2 = \langle r^4\rangle/\langle r^2\rangle$ and $\hat{w}$ has the following form.

$$\hat{w} = \frac{\partial}{\partial\psi}\left(\hat{\rho}\langle r^2\rangle\frac{\partial\Phi}{\partial\psi}\right) + \frac{\partial}{\partial\varphi}\left(\hat{\rho}\left\langle\frac{1}{r^2B^2} + \lambda^2B^2\right\rangle\frac{\partial\Phi}{\partial\varphi}\right) \quad (2)$$

where $\Phi \equiv c\phi$, c light speed, ϕ electrostatic potential, w is related to the specific volume averaged vorticity $\nabla\times(\rho c\boldsymbol{B}\times\nabla\phi/B^2)$ due to plasma $\boldsymbol{E}\times\boldsymbol{B}$ drift flux, and v_α^2 is the square of plasma fluid velocity. Poisson bracket is defined as

$$[\![\Phi, \hat{w}]\!] \equiv \frac{\partial\Phi}{\partial\psi}\frac{\partial\hat{w}}{\partial\varphi} - \frac{\partial\Phi}{\partial\varphi}\frac{\partial\hat{w}}{\partial\psi} \quad (3)$$

author's e-mail: katanuma@prc.tsukuba.ac.jp

The second term in the right hand side in eq.(1) represents the viscosity of fluid and the third term contains the effects that the vorticity can move along a magnetic null.

The transport equations of mass density and heat are given in the following on the assumption of the adiabatic index $\gamma = 5/3$.

$$\frac{\partial \hat{\rho}_0}{\partial t} - \frac{\partial}{\partial \psi}\left(\overline{\tilde{\rho}\frac{\partial \Phi}{\partial \varphi}}\right) = 4\pi d_M \frac{\partial}{\partial \psi}\left[\frac{\hat{\rho}_0\langle r^2\rangle U}{\hat{T}_0^{3/2}}\frac{\partial}{\partial \psi}\left(\frac{\hat{\rho}_0\hat{T}_0}{U^{5/3}}\right)\right] + \overline{Q}_\rho^* U \quad (4)$$

$$\frac{\partial \tilde{\rho}}{\partial t} + [\![\Phi, \tilde{\rho}]\!] + \frac{\partial}{\partial \psi}\left(\overline{\tilde{\rho}\frac{\partial \Phi}{\partial \varphi}}\right) - \frac{\partial \Phi}{\partial \varphi}\frac{\partial \hat{\rho}_0}{\partial \psi} = \tilde{Q}_\rho^* U + 4\pi d_M \times \left(\frac{\partial}{\partial \psi}\left[\frac{\hat{\rho}_0\langle r^2\rangle U}{\hat{T}_0^{3/2}}\frac{\partial}{\partial \psi}\left(\frac{\tilde{\rho}\hat{T}_0}{U^{5/3}}\right)\right] + \left[\frac{\hat{\rho}_0}{\hat{T}_0^{1/2}U^{2/3}}\left\langle\frac{1}{r^2B^2}\right\rangle\frac{\partial^2 \tilde{\rho}}{\partial \varphi^2}\right]\right) \quad (5)$$

$$\frac{\partial \hat{T}_0}{\partial t} - \frac{\partial}{\partial \psi}\left(\overline{\tilde{T}\frac{\partial \Phi}{\partial \varphi}}\right) = X_M \frac{2U^{2/3}}{3\hat{\rho}_0}\frac{\partial}{\partial \psi}\left(\frac{\hat{\rho}_0^2\langle r^2\rangle}{U}\frac{\partial}{\partial \psi}\left(\frac{\sqrt{\hat{T}_0}}{U^{1/3}}\right)\right) + \frac{8\pi d_M}{3\sqrt{\hat{T}_0}}\frac{\partial}{\partial \psi}\left(\langle r^2\rangle U\frac{\partial}{\partial \psi}\left(\frac{\hat{\rho}_0\hat{T}_0}{U^{5/3}}\right)\right) + \frac{U^{5/3}}{\hat{\rho}}\overline{Q}_T^* \quad (6)$$

$$\frac{\partial \tilde{T}}{\partial t} + [\![\Phi, \tilde{T}]\!] + \frac{\partial}{\partial \psi}\left(\overline{\tilde{T}\frac{\partial \Phi}{\partial \varphi}}\right) - \frac{\partial \Phi}{\partial \varphi}\frac{\partial \hat{T}_0}{\partial \psi} = \frac{U^{5/3}}{\hat{\rho}}\tilde{Q}_T^* + X_M\frac{U^{2/3}}{3\hat{\rho}_0} \times \frac{\partial}{\partial \psi}\left(\frac{\hat{\rho}_0^2\langle r^2\rangle}{U}\frac{\partial}{\partial \psi}\left(\frac{\tilde{T}}{U^{1/3}\sqrt{\hat{T}_0}}\right)\right) + \frac{X_M\hat{\rho}_0}{3U^{2/3}\sqrt{\hat{T}_0}}\left\langle\frac{1}{r^2B^2}\right\rangle\frac{\partial^2 \tilde{T}}{\partial \varphi^2} \quad (7)$$

Here $\rho \equiv M_i n_i + M_e n_e = \langle\rho\rangle \equiv \hat{\rho}/U$ is mass density. The slow time variable equilibrium component $\hat{\rho}_0(\epsilon^3 t, \psi)$ and fast variable fluctuating components $\tilde{\rho}(\epsilon t, \psi, \varphi)$ are defined, where the equilibrium quantity is represented by the hat with subscript $\hat{}_0$ and fluctuating quantity is by the tilde $\tilde{}$, i.e. and $\hat{\rho} = \hat{\rho}_0 + \tilde{\rho}$. The quantity $\hat{T}$ is related to the temperature defined by $\hat{T} \equiv pU^\gamma/\hat{\rho} = (T_i + T_e)U^{\gamma-1}/M_i$. The symbol $\overline{A}$ means the average of A over φ, $\hat{A}$ means the quantity of A integrated in the specific volume of a magnetic field line, and the symbol $\langle A\rangle$ means the integration of A along a magnetic field lines,

$$\overline{A} \equiv \frac{1}{2\pi}\int_0^{2\pi} A\,\mathrm{d}\varphi\,, \quad \hat{A} \equiv \int \frac{A\,\mathrm{d}\zeta}{J(\psi,\varphi,\zeta)}\,, \quad \langle A\rangle \equiv \frac{\hat{A}}{U} \quad (8)$$

where $J(\psi,\varphi,\zeta) \equiv \nabla\psi\times\nabla\varphi\cdot\nabla\zeta$ is Jacobian. The magnetic field line curvatures are included in the coefficients U, $\langle r^2\rangle$, $\langle\frac{1}{r^2B^2}\rangle$ in the eqs.(1)-(7), and the definition of U is

$$U \equiv \int \frac{\mathrm{d}\zeta}{J(\psi,\varphi,\zeta)} \quad (9)$$

The coordinates (ψ,φ,ζ) adopted here are the flux coordinates, where magnetic field is represented as $\boldsymbol{B} = \nabla\psi\times\nabla\varphi$. Here $2\pi\psi$ gives the magnetic flux inside the surface of $\psi = const$, and φ corresponds to an angle coordinate. The remaining coordinate ζ is usually taken as z-axis or along magnetic field line.

The classical diffusions included in eqs.(1)-(7) are defined by

$$X_M = \chi_\perp\frac{B^2}{\rho}\left(\frac{4T_i}{T_i+T_e}\right)\left(\frac{p}{\rho}\right)^{1/2}$$
$$d_M = \frac{m_e^{1/2}(T_i+T_e)T_i^{1/2}}{\sqrt{2}m_i^{1/2}T_e^{3/2}}\left(\frac{B^2}{4\pi\rho}\left(\frac{p}{\rho}\right)^{1/2}\chi_\perp\right) \quad (10)$$

$$\chi_\perp = \frac{T_i}{m_i\omega_{ci}^2\tau_i}\,, \qquad \epsilon^3 \equiv \frac{\chi_\perp}{bc_s}\left(\frac{2T_i}{T_i+T_e}\right) \quad (11)$$

Here τ_i is the classical ion-ion coulomb collision time[5], $c_s \equiv \sqrt{\gamma p/\rho}$ is the ion sound speed , and b is a distance defined by $b \equiv \sqrt{\psi_b/B_M}$, where the subscript $_M$ means some axial position on axis. The quantities related to classical transport X_M and d_M in eq.(10) are the dimensionless quantities which are constant along a magnetic field line. The mass density ρ and other plasma quantities T_e, T_i are assumed to be constant along a magnetic field line through this paper. The parameter ϵ defined in eq.(11) is a small expansion parameter, where we assume $\epsilon^2 = 10^{-2}$ in the numerical calculation of next section in this paper.

The basic equations in this section contain the interchange modes (similar to the Rayleigh-Taylor instabilities) and the modes associated with the presence of nonuniform plasma flows (similar to the Kelvin-Helmholtz instabilities) as well as the electrostatically incompressible stable plasma flows. So this close set of equations describe the nonlinear low-frequency MHD plasma convection and resulting transport processes in weakly dissipative plasmas in axisymmetric shearless systems.

3. Numerical results

Numerical calculation by using the basic equations (1)-(7) is carried out in the magnetic divertor shown in Fig.1 for the purpose of investigating the effects of flute mode fluctuations on the plasma radial transport.

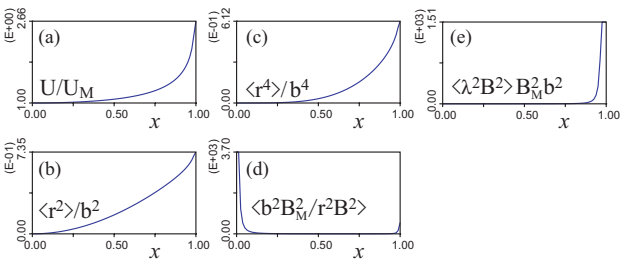

Fig. 2 Basic parameters of magnetic divertor.

The geometrical parameters of the magnetic divertor in Fig.1 are plotted in Fig.2, where the specific volume $u \equiv U/U_M$ in (a), $\langle r^2\rangle/b^2$ in (b), $\langle r^4\rangle/b^4$ in (c), $\langle\frac{1}{r^2B^2}\rangle B_M^2 b^2$ in (d), and $\langle\lambda^2B^2\rangle B_M^2 b^2$ as a function of $x \equiv \sqrt{\psi/\psi_b}$. The classical diffusion coefficients of quasi-equilibrium ($m = 0$) density and temperature are proportional to $\langle r^2\rangle$ in eqs.(4) and (6), which have maximum values at $x = 1$ in Fig.2(b). The classical diffusion coefficients of the perturbed components ($m \neq 0$) of vorticity and temperature in the φ direction are proportional to $\langle r^4\rangle\langle\frac{1}{r^2B^2} + \lambda^2B^2\rangle/\langle r^2\rangle^2$ and $\langle\frac{1}{r^2B^2}\rangle$ in eqs.(1) and (7), which diverge at the axis in Fig.2(d). The effects that fluid can flow freely in the azimuthal direction along a magnetic null line are included through $\langle\lambda^2B^2\rangle$ in eqs.(1) and (2). The potential Φ is determined by eq.(2). A dimensionless parameter ϵ in eq.(11) contains the magnitude of the classical diffusion.

The equations (1)-(7) have the steady state solutions if the classical diffusion is neglected, i.e. $\epsilon = 0$, that is

$$\hat{\rho}_0(\psi) = const.\,, \quad \hat{T}_0(\psi) = const.\,, \quad \hat{w}_0(\psi) = const. \quad (12)$$

The field line integrated vorticity $w_0 = -1$ gives a plasma azimuthal rigid rotation so that there is no shear flow in this initial condition. As long as eq.(12) is satisfied any fluctuations do not generate in eqs.(1)-(7). So we add a small fluctuation $\tilde{T}$ to the initial condition eq.(12), i.e. $\hat{\rho}_0 = 1$, $\hat{T}_0 = 1$, $\hat{w}_0 = -1$, in the following numerical calculation, where the initial perturbation $\tilde{T}$ added to equilibrium temperature $\hat{T}_0$ is plotted in Fig.3(b).

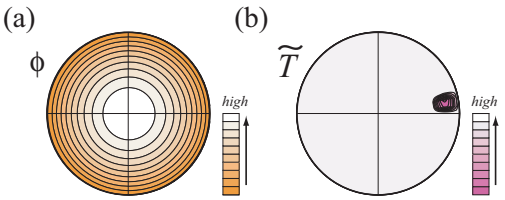

Fig. 3 Initial condition of ϕ and $\tilde{T}$.

Henceforth, the normalized time τ defined as $\tau = \frac{\epsilon c_{sM}}{b} t$ is introduced. The specific volume averaged perturbed quantity $\widetilde{A}$ is plotted in place of $\tilde{A}$ in the following figures. The initial condition $\hat{w}_0 = -1$ gives the axisymmetric potential profile shown in Fig.3(a), where the plasma rotates clockwise rigidly around axis at the amount of 2π during $\tau \simeq 4$. This initial condition is unstable to the flute modes.

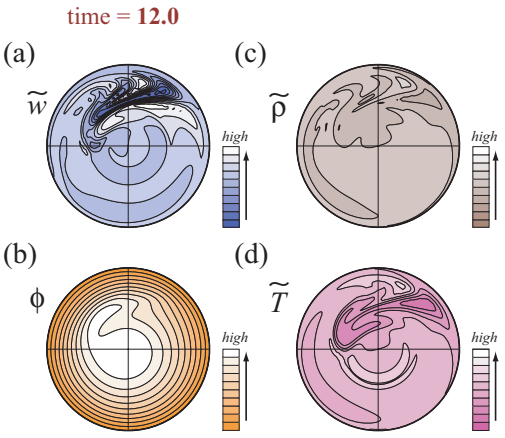

Fig. 4 The potential and the perturbed quantities at $\tau = 12$.

The flute modes grow in a linear phase with the rotation of plasma around axis by $\boldsymbol{E}\times\boldsymbol{B}$-drift, and then the first big flute instability appears at $\tau = 12$ in Fig.4. A typical parasol shaped equi-contour surfaces to Rayleigh-Taylor instabilities of $\widetilde{T} \equiv \tilde{T}/U^{2/3}$ can be seen in Fig.4(d)

The radial profiles and radial fluxes Γ_ρ of mass density and Γ_T of temperature are plotted at $\tau = 12$ in Fig.5. Initial flux volume integrated mass density $\hat{\rho}_0 = \rho_0 U$ and temperature $\hat{T}_0 = T_0 U^{2/3}$ profiles are close to the initial profiles except for the region $x \simeq 1$ where the classical radial flux dominates in Figs.5(e) and (f). In the region where flute instability occurs, the anomalous radial fluxes are much larger than the classical ones in Figs.5(e) and (f). The plasma rotates clockwise in whole region as seen in Figs.5(b) where the potential has a monotonously decreas-

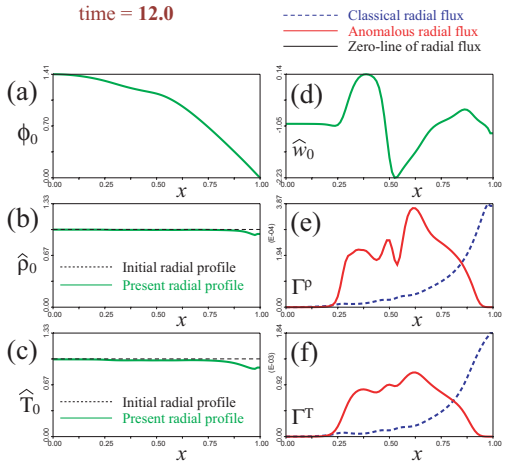

Fig. 5 Radial profiles of ϕ_0, $\hat{\rho}_0$, $\hat{T}_0$, $\hat{w}_0$ and radial fluxes of mass density Γ_ρ and temperature Γ_T at $\tau = 12$.

ing radial profile. In the region $x \lesssim 0.25$, where the flute modes do not reach yet, classical transport dominates and plasma rotates rigidly in the azimuthal direction. The parasol shaped low temperature region generated by the flute instability in Fig.4 continues in $\tau \simeq 10$ and then disappears.

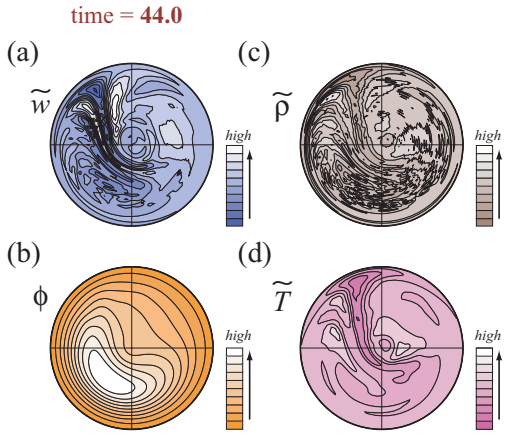

Fig. 6 The potential and the perturbed quantities at $t = 44$.

The flute instabilities appear and disappear repeatedly in time with enhancing radial transport during the existence of the instabilities. Figure 6 plots the profiles of perturbation quantities at $\tau = 44$. The potential has a peak off axis at that time in Fig.6(b). The low temperature region penetrates at axis in Fig.6(d) which is accompanied by the penetration of the low density region in Fig.6(c). Many short wave length perturbations are seen in mass density $\widetilde{\rho}$ than that in temperature $\widetilde{T}$ because the modes associated with the presence of nonuniform plasma flows (similar to the Kelvin-Helmholtz instabilities) grows in mass density where the classical diffusion coefficient of mass density in eq.(5) is much smaller than that of the temperature in eq.(7).

The radial profile of potential ϕ_0 has a maximum at

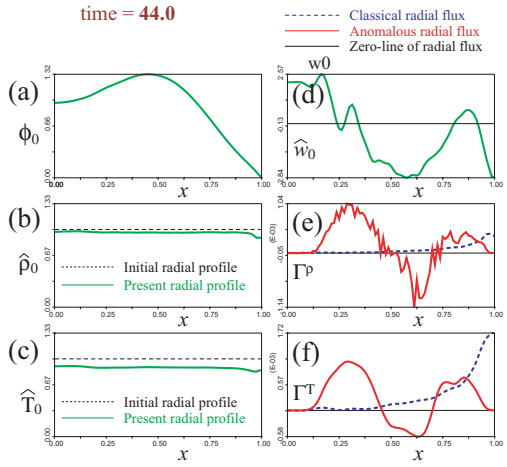

Fig. 7 Radial profiles of ϕ_0, $\hat{\rho}_0$, $\hat{T}_0$, $\hat{w}_0$ and radial fluxes of mass density Γ_ρ and temperature Γ_T at $\tau = 44$.

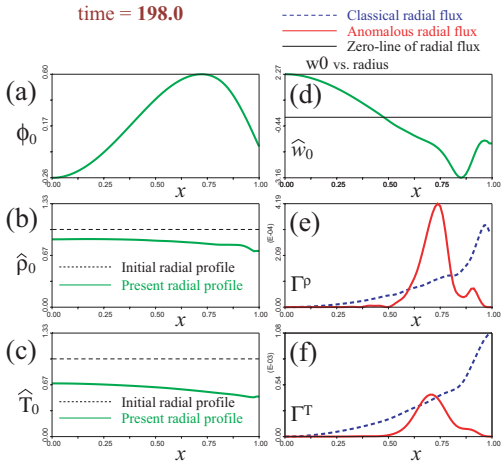

Fig. 9 Radial profiles of ϕ_0, $\hat{\rho}_0$, $\hat{T}_0$, $\hat{w}_0$ and radial fluxes of mass density Γ_ρ and temperature Γ_T at $\tau = 198$.

$x \simeq 0.45$ at $\tau = 44$ in Fig.7(a). That is, two counter flows exist at this time. Fig.7(d) plots the radial profile of w_0, maximum and minimum values of which are 2.57 and -2.87, respectively. These magnitudes are larger than the initial magnitude of w_0. Because the total vorticity is conserved in this simulation, there is inward transport of angular momentum. In the region $0.1 < x < 0.8$ the enhanced radial transport exists and the plasma shakes forward and backward radially as shown in Figs.7(e) and (f).

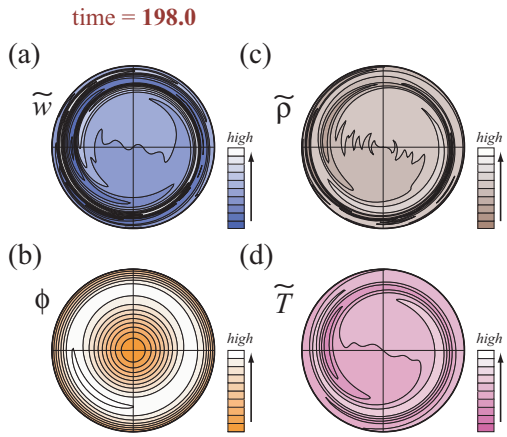

Fig. 8 The potential and the perturbed quantities at $t = 198$.

The system comes to a quasi-steady state after the long run as shown in Fig.8, in the meaning that the structures do not change so much in time. In this state any perturbations are not observed in the region $x \lesssim 0.6$ in Fig.8. Although the potential in Fig.8(b) has almost axisymmetric profile, its radial profile is not constant shown in Fig.9(a). The radial profile w_0 is also not constant radially, which means that there are shear flows (not rigid rotation).

In the region $x \gtrsim 0.6$ in Fig.8 the vortex structures of $\widetilde{w}, \widetilde{\rho}, \widetilde{T}$ are seen, where the anomalous radial transports are enhanced in ρ_0 and T_0 in Fig.9(e) and (f). The equilibrium quantities of $\hat{\rho}_0$ and $\hat{T}_0$ shown in Fig.9(b) and (c) has a flatter slope in the region $x \lesssim 0.5$ than those in $x \gtrsim 0.5$, which reminds us of the transport barrier observed in toroidal confinement systems. However, these radial profiles decreases radially so that the system is unstable to the flute modes when without counter shear flows. That is, Figs.8 and 9 show that the counter shear flows prevent the flute modes from being unstable.

5. Summary

We made a computer code using the basic equations obtained in Ref.4. These equations exclude the shear Alfvén modes and compressional modes from MHD equations in order to follow the flute modes and the instability driven by nonuniform plasma flows (similar to the Kelvin-Helmholtz instabilities). We carried out the computer simulation in a modeled divertor mirror cell in the initial condition with finite rigid rotation but no shear flows.

Initial small temperature dip around the outer boundary causes the flute instabilities. The flute instabilities are accompanied by the large enhanced radial transport of mass density and temperature. At the end of the computer simulation, the counter shear flow appears which suppresses the anomalous radial transport as something like transport barrier formation. The equilibrium mass density and temperature have profiles decreasing radially, which should be unstable to flute modes, continue to be stable under the existence of counter shear flows.

[1] I.Katanuma, Y.Sasagawa, Y.Tatematsu, Y.Nakashima, T.Cho, V.P.Pastukhov, Nucl. Fusion, **46**, 608 (2006).
[2] Y.Sasagawa, I.Katanuma, Y.Mizoguchi, T.Cho, V.P.Pastukhov, Phys. Plasmas, **13**, 122506 (2006).
[3] I.Katanuma, Y.Tatematsu, K.Ishii, T.Tamano, K.Yatsu, J. Phys. Soc. Jpn., **69**, 3244(2000).
[4] P.V.Pastukhov 2005 Plasma Phys. Rep. **31**, 577.
[5] S.I.Braginskiin *Reviews of Plasma Physics*, ed. A.M.A.Leontovich (Consultants Bureau, New York, 1965) Vol. 1.